Thermodynamically Reversible Addressing of a Stimuli Responsive Fusion Protein onto a Patterned Surface Template†

Wolfgang Frey,*,‡ Dan E. Meyer, and Ashutosh Chilkoti*

Department of Biomedical Engineering, Duke University, Campus Box 90281, Durham, North Carolina 27708-0281

Received August 5, 2002. In Final Form: November 17, 2002

The sensitivity of an elastin-like polypeptide (ELP) to environmental stimuli is used to reversibly immobilize a fusion partner, thioredoxin (TRX), onto a hydrophobic surface. An ELP, fused to TRX at its C-terminus, adsorbs onto a hydrophobic self-assembled monolayer (SAM) on gold above its inverse phase transition temperature (T_c) and is resolubilized from the surface when the solution temperature is lowered below T_c. We show that the adsorbed fusion partner TRX is recognized by an antibody specific to TRX and that the complex is also resolubilized from the surface below T_c. Adsorption of TRX−ELP is inhibited by hydrophilic surfaces that are defect-free. In situ ellipsometry shows that the ELP-anchored TRX adsorbs above T_c up to a well-defined layer thickness that is greater than a monolayer and that the adsorption and desorption cycle can be repeated. These results are confirmed by atomic force microscopy and by surface plasmon resonance spectroscopy. The preferential adsorption of TRX−ELP on hydrophobic surfaces is used to create a pattern of adsorbed protein on a surface composed of a pattern of hydrophobic and hydrophilic SAMs on gold. We term this method to reversibly address an ELP fusion protein to chemically distinct regions of a patterned surface by an external stimulus "thermodynamically reversible addressing of proteins" (TRAP).

1. Introduction

Patterned biomolecules on surfaces have many applications, ranging from the modulation of cell−substrate interactions in biomaterials and tissue engineering[1−12] to the fabrication of multianalyte biosensors,[13] clinical assays, and genomic[14] and proteomic arrays.[15−17] A variety of methods exist to pattern biomolecules on different substrates, such as metals,[18−22] polymers,[23] and glass.[24] Often the first step in achieving patterned biomolecules involves a surface modified with a self-assembled monolayer (SAM), which can be patterned by photolithography[13] or by an ensemble of techniques that are collectively termed soft lithography.[25,26] These surfaces are then used as the template for the subsequent patterning by spatially selective adsorption of the biomolecule, by covalent conjugation of the biomolecule, or by molecular recognition between the biomolecule and its ligand, which has itself been patterned on the SAM.[27]

For many applications, it would be useful to be able to address a specific region of the surface selectively with a biomolecule from solution, to immobilize the biomolecule at the predetermined address without chemical intervention so as to present the biomolecule in a functionally active orientation, and finally to remove the biomolecule or its noncovalent complex with a binding partner from the address on the surface. Despite the diversity of protein patterning methods available, most of these methods

* To whom correspondence should be addressed. Ashutosh Chilkoti: tel, (919) 660-5373; fax, (919) 660-5362; e-mail, chilkoti@duke.edu. Wolfgang Frey: tel, (512) 471-7434; e-mail, wfrey@mail.utexas.edu.

† Part of the *Langmuir* special issue entitled The Biomolecular Interface.

‡ W.F. is now at the Department of Biomedical Engineering, University of Texas at Austin, Mailcode C0800, Austin, TX 78712. E-mail: wfrey@mail.utexas.edu. Tel: (512) 471-7434.

(1) Fromherz, P.; Schaden, H.; Vetter, T. *Neurosci. Lett.* **1991**, *129*, 77−80.
(2) Chen, C. S.; Mrksich, M.; Huang, S.; Whitesides, G. M.; Ingber, D. E. *Science* **1997**, *276*, 1425−1428.
(3) Craighead, H. G.; James, C. D.; Turner, A. M. P. *Curr. Opin. Solid State Mater. Sci.* **2001**, *5*, 177−184.
(4) Scotchford, C. A.; Cooper, E.; Leggett, G. J.; Downes, S. *J. Biomed. Mater. Res.* **1998**, *41*, 431−442.
(5) Singhvi, R.; Kumar, A.; Lopez, G. P.; Stephanopoulos, G. N.; Wang, D. I. C.; et al. *Science* **1994**, *264*, 696−698.
(6) Desai, T. A. *Med. Eng. Phys.* **2000**, *22*, 595−606.
(7) Kasemo, B. *Curr. Opin. Solid State Mater. Sci.* **1998**, *3*, 451−459.
(8) Dillow, A. K.; Tirrell, M. *Curr. Opin. Solid State Mater. Sci.* **1998**, *3*, 252−259.
(9) Jung, D. R.; Kapur, R.; Adams, T.; Giuliano, K. A.; Mrksich, M.; et al. *Crit. Rev. Biotechnol.* **2001**, *21*, 111−154.
(10) Folch, A.; Toner, M. *Annu. Rev. Biomed. Eng.* **2000**, *2*, 227.
(11) Castner, D. G.; Ratner, B. D. *Surf. Sci.* **2002**, *500*, 28−60.
(12) Prokop, A. In *Bioartificial Organs III*: *Tissue Sourcing, Immunoisolation, and Clinical Trials*; Hunkeler, D., Cherrington, A., Prokop, A., Rajotte, R., Eds.; Annals of the New York Academy of Sciences Vol. 944; New York Academy of Sciences: New York, 2001; pp 472−490.
(13) Blawas, A. S.; Reichert, W. M. *Biomaterials* **1998**, *19*, 595−609.
(14) Schena, M.; Davis, R. W. In *Microarray Biochip Technology*; Schena, M., Ed.; Eaton Publishing: Natick, MA, 2000; pp 1−18.
(15) Mirzabekov, A.; Kolchinsky, A. *Curr. Opin. Chem. Biol.* **2001**, *6*, 70−75.
(16) Houseman, B. T.; Huh, J. H.; Kron, S. J.; Mrksich, M. *Nat. Biotechnol.* **2002**, *20*, 270−274.
(17) Wilson, D. S.; Nock, S. *Curr. Opin. Chem. Biol.* **2002**, *6*, 81−85.
(18) Kumar, A.; Biebuyck, H. A.; Whitesides, G. M. *Langmuir* **1994**, *10*, 1498−1511.
(19) Folkers, J. P.; Gorman, C. B.; Laibinis, P. E.; Buchholz, S.; Whitesides, G. M.; Nuzzo, R. G. *Langmuir* **1995**, *11*, 813−824.
(20) Yousaf, M. N.; Houseman, B. T.; Mrksich, M. *Proc. Natl. Acad. Sci. U.S.A.* **2001**, *98*, 5992−5996.
(21) Wilson, D. L.; Martin, R.; Hong, S.; Cronin-Golomb, M.; Mirkin, C. A.; Kaplan, D. L. *Proc. Natl. Acad. Sci. U.S.A.* **2001**, *98*, 13660−13664.
(22) Patel, N.; Bhandari, R.; Shakesheff, K. M.; Cannizzaro, S. M.; Davies, M. C.; et al. *J. Biomater. Sci., Polym. Ed.* **2000**, *11*, 319−331.
(23) Yang, Z. P.; Chilkoti, A. *Adv. Mater.* **2000**, *12*, 413−417.
(24) Xia, Y. N.; Mrksich, M.; Kim, E.; Whitesides, G. M. *J. Am. Chem. Soc.* **1995**, *117*, 9576−9577.
(25) Xia, Y. N.; Whitesides, G. M. *Angew. Chem., Int. Ed.* **1998**, *37*, 551−575.
(26) Whitesides, G. M.; Ostuni, E.; Takayama, S.; Jiang, X. Y.; Ingber, D. E. *Annu. Rev. Biomed. Eng.* **2001**, *3*, 335−373.
(27) Ostuni, E.; Yan, L.; Whitesides, G. M. *Colloids Surf., B* **1999**, *15*, 3−30.

10.1021/la026359d CCC: $25.00
Published on Web 01/23/2003

result in static patterns, that is, patterns that cannot be dynamically controlled or modulated after fabrication. To create dynamic patterns of biomolecules on surfaces, one approach is to create surfaces with patterned chemical reactivity that can be switched on and off locally. Approaches to switch on a functionality in situ have been realized using SAMs with caged functional groups[28] or with an electroactive functionality based on hydroquinone conjugates.[20,29] This approach is attractive but has two limitations: first, the chemistry required to alter the reactivity of the surface has to be carried out in an aqueous environment under conditions that are compatible with biological molecules. Second, once the functionality is created it cannot easily be reversed.

We recently demonstrated proof-of-principle of an alternative method, thermodynamically reversible addressing of proteins (TRAP), to dynamically address proteins onto micropatterned surface templates by modulating the interaction between a patterned surface and a recombinant stimuli responsive fusion protein.[30] Here we present quantitative results of the TRAP process. We chose thioredoxin (TRX) as the fusion protein because it expresses at high levels from a plasmid-borne gene in *Escherichia coli* and has good solubility and stability.[31,32] The fusion protein is stimuli responsive because it has a C-terminal elastin-like polypeptide (ELP) tail that undergoes a reversible phase transition in response to external stimuli such as a change in temperature, ionic strength, or pH.[33] This demixing transition, termed the inverse transition in the biopolymer literature, is characterized by the desolvation and aggregation of the polypeptide at a critical solution temperature,[34−36] a phenomenon that has also been observed for synthetic polymers such as poly(*N*-isopropyl acrylamide).[37] In TRAP, the external stimulus triggers the interaction of the stimuli responsive ELP tail with specified regions of a micropatterned surface template. Furthermore, the fusion protein is functionally unaffected by the trigger[33] and is bound to the surface in an orientation that enables binding of its ligand from solution by molecular recognition. The resulting pattern of the noncovalent complex of the ELP fusion protein and its ligand is desorbed when the external trigger is reversed. Because binding and desorption can be dynamically switched on and off in TRAP, this patterning approach is conceptually analogous to an electronic data storage chip (RAM), in that the processes of addressing, writing, reading, and erasing are implemented by a spatially selective trigger, adsorption, molecular recognition, and resolubilization, respectively.

This paper is organized in three parts. Part one, the dynamic control of the immobilization, describes the process by which an ELP fusion protein can be reversibly immobilized on a hydrophobic surface, based on the inverse phase transition of the ELP. We also demonstrate that the adsorption of an ELP fusion protein by the external trigger is negligible on a hydrophilic surface. Part two, the dynamic control of surface functionalization, describes the accessibility of the immobilized fusion partner, TRX, to binding of a monoclonal antibody specific to TRX. Part three, the dynamic patterning, demonstrates the reversible addressing of the TRX−ELP fusion protein to selected areas on a patterned surface, composed of hydrophobic regions against a hydrophilic background, by exploiting the preferential binding of TRX−ELP to a hydrophobic surface as compared to a hydrophilic surface.

2. Experimental Section

2.1. Surface Preparation. Gold surfaces were prepared on cleaned silicon wafers by evaporation of 30−50 Å of Cr followed by 1800−2000 Å of gold (both Alpha Aesar) in a thermal evaporator at evaporation rates of about 5 Å/s. Directly before use of the samples, the gold surfaces were cleaned in water (≥18 MΩ)/ammonium hydroxide/hydrogen peroxide (both EM Science) (5:1:1) at 80 °C for 5 min, rinsed with water, and dried under a stream of N_2.

Hydrophobic surfaces were created by incubating freshly cleaned gold surfaces in a 1 mM solution of hexadecanethiol (HDT) (Aldrich) in ethanol absolute (Aldrich) for at least 20 h. Samples were then sonicated for 1 min in ethanol absolute, dried under a stream of N_2, and used immediately. Hydrophilic surfaces were created by incubating freshly cleaned surfaces in a 1 mM solution of mercaptoundecanoic acid (MUDA) (Aldrich) in ethanol absolute/water/acetic acid (EM Science) (85:10:5 v/v/v) for at least 20 h. Samples were removed from the solvent bath and sonicated in the solvent mixture for 1 min, followed by 1 min sonication in 0.1 M HCl and 1 min sonication in water, and were then dried under a stream of N_2.

Patterned surfaces were prepared using microcontact printing (μCP).[38] Poly(dimethylsiloxane) (PDMS) stamps were created from photoresist on silicon masters with positive relief features of lines and interfeature spacing, both nominally of 40 μm. The PDMS stamps were inked with a 1 mM solution of HDT in ethanol absolute using a Q-Tip and dried under N_2. The stamps were brought into contact with the freshly cleaned gold surface for 2 min after which the gold surface was dried under N_2.[39] Samples were then immediately incubated in a solution of MUDA in the solvent mixture described above for about 12 h, after which they were cleaned using the procedure described for MUDA monolayer SAMs, and used immediately.

2.2. Synthesis of the Thioredoxin−ELP Fusion Protein. An ELP with a molecular weight of 71 000 Da was used for all experiments. It consists of 18 repeats of 10 VPGXG pentapeptides, that is, each containing 50 amino acids (AA) of VPGXG. The sequence of the fourth residue (X) in the 10 pentapeptides is V-V-G-A-V-V-V-G-A-G. This ELP was fused to the C-terminus of TRX, which has a molecular weight of 14 000, as described previously.[33] In brief, a synthetic ELP gene encoding 10 pentapeptides was oligomerized recursively (in pUC-19)[40] up to a gene encoding 400 AA. The gene was excised from pUC-19, fused at the 3′-end of the TRX gene, contained in the pET-32b vector (Novagen), and transformed in *E. coli* strain BLR(DE3). The gene was induced by IPTG in shaker flask cultures of BLR(DE3) harboring the expression plasmid, and the soluble TRX−ELP was isolated from contaminating *E. coli* proteins by four rounds of inverse transition cycling.[33] Each round of inverse transition cycling involved aggregation of the soluble fusion protein at room temperature by the addition of 4 M NaCl, centrifugation at 2000*g* for 5 min to pellet the aggregated fusion protein, resuspension of the protein pellet in 50 mM phosphate buffer and 0.15 M NaCl, pH 7.4, at 4 °C, and centrifugation at 10000*g* at 4 °C for 2 min to remove insoluble precipitates. After the concentration was determined by UV−vis absorption spectroscopy, the protein was stored in individual aliquots for each experiment in 50 mM potassium phosphate and 0.15 M NaCl, pH 7.4, at −80 °C until further use.

(28) Yang, Z. P.; Frey, W.; Oliver, T.; Chilkoti, A. *Langmuir* **2000**, *16*, 1751−1758.
(29) Yousaf, M. N.; Mrksich, M. *J. Am. Chem. Soc.* **1999**, *121*, 4286−4287.
(30) Frey, W.; Meyer, D. E.; Chilkoti, A. *Adv. Mater.*, accepted.
(31) Katti, S. K.; LeMaster, D. M.; Eklund, H. *J. Mol. Biol.* **1990**, *212*, 167−184.
(32) Santoro, M. M.; Bolen, D. W. *Biochemistry* **1992**, *31*, 4901−4907.
(33) Meyer, D. E.; Chilkoti, A. *Nat. Biotechnol.* **1999**, *17*, 1112−1115.
(34) Urry, D. W. *J. Protein Chem.* **1984**, *3*, 403−436.
(35) Urry, D. W. *Prog. Biophys. Mol. Biol.* **1992**, *57*, 23−57.
(36) Urry, D. W. *J. Phys. Chem. B* **1997**, *101*, 11007−11028.
(37) Schild, H. G. *Prog. Polym. Sci.* **1992**, *17*, 163−249.
(38) Kumar, A.; Whitesides, G. M. *Appl. Phys. Lett.* **1993**, *63*, 2002−2004.
(39) Libioulle, L.; Bietsch, A.; Schmid, H.; Michel, B.; Delamarche, E. *Langmuir* **1999**, *15*, 300−304.
(40) Meyer, D. E.; Chilkoti, A. *Biomacromolecules* **2002**, *3*, 357−367.

2.3. Solution Preparation. All solutions were prepared with 50 mM potassium phosphate, pH 7.4, ultrapure water with a resistivity of >18 MΩ, and varying NaCl concentrations. Stock solutions containing 0.15, 1.25, and 4 M NaCl were each cleaned with chloroform and then extracted with hexane to remove impurities from the salt. Other salt concentrations were mixed from these stocks at the time of use. The 50 mM phosphate buffer, pH 7.4, and 1.25 M NaCl is referred to in the text as the standard buffer.

2.4. Dynamic Light Scattering. Dynamic light scattering (DLS) was performed in a DynaPro-LSR dynamic light scattering instrument (Protein Solutions, Charlottesville, VA) equipped with a Peltier temperature control unit. Buffers were filtered through a 0.02 μm Anodisc (Whatman) filter before adding protein to a final concentration of 1 μM. Autocorrelation functions were measured at nonequidistant temperature intervals as the solution was heated from 10 to 40 °C. Data were obtained at each temperature by ramping the cell up to the temperature of interest, allowing the sample to equilibrate for 10 min, and collecting three sets of 25 autocorrelation functions each, separated by 5 min. Analysis of the autocorrelation function, to determine the hydrodynamic radius (R_h), was performed using Protein Solutions' Dynamics software. Conversion into particle number was performed by customized software using Mie theory for spheres, assuming a refractive index of 1.40, which is only important for R_h > 200 nm.

2.5. In Situ Ellipsometry. An ellipsometer, built in-house, was used for all ellipsometric measurements. The ellipsometer consists of a 10 mW HeNe laser (Melles Griot), two quarter wave plates (Newport), two polarizers mounted in continuous rotators with <1/100° absolute accuracy (Newport), a home-built detector with preamplifier, and a lock-in amplifier (PAR, EG&G). The ellipsometric angles were determined by nulling the intensity in a PCSA (polarizer−compensator−sample−analyzer) setup[41] with a compensator at $\pi/4$ at an angle of incidence of 68.25°. Imaging ellipsometry was performed with the same setup, except that two lenses were introduced in the output arm and the detector was replaced with a CCD camera (Dage MTI) and a frame grabber. The camera's gain and black level were kept constant, and in some cases a neutral density filter was placed in front of the camera to avoid saturation.

Samples were mounted in a glass cuvette with entrance and exit windows perpendicular to the beam, placed on a small goniometer table with a small stirrer. Stress-induced birefringence was minimized by using silicon rubber to glue the glass pieces together during fabrication of the cuvette and by using 3 mm thick entrance and exit windows made from fused silica. A recirculating water coil, connected to a Neslab RTE-111 recirculating water bath, and a small stir bar placed in the cuvette allowed the temperature in the cuvette to be homogeneously controlled to 0.1 °C accuracy. A resistor temperature sensor inserted into the cuvette allowed measurement of the in situ temperature of the solution.

The refractive index of the experimental buffer was determined for different NaCl concentrations at different temperatures on a Bellingham Stanley RFM 340 refractometer. The experimentally determined refractive indices were fitted, and the formula

$$1.3367 - 0.00010578T - (6.3401 \times 10^{-7})T^2 + 0.009665C$$

with C being the salt concentration in molar units and T being the buffer temperature in °C, was used to determine refractive indices over the range of temperatures and salt concentrations used in the in situ ellipsometry measurements. Our data for water are identical to within 0.0001 to those found by Franko[42] and within 0.0003 to those in reference tables,[43] and also better than ±0.001 in agreement with several sources at around room temperature for buffers of different NaCl concentrations.[42,44]

The complex refractive index of gold was determined for each newly prepared wafer and was assumed to be constant for the whole wafer. Values of $n = 0.20 - i\,3.558$ agree well with literature values for evaporated gold films.[45] The optical properties of additional layers were assumed to not be influenced by the typical roughness of thermally evaporated gold, which is a valid assumption as long as the adsorbed film follows the contours of the gold surface.[46] The polarizer and analyzer angles were always measured in two quadrants, and the average of the two measurements determined the ellipsometric parameters, which are defined as

$$\frac{R_p}{R_s} = \tan(\Psi)e^{i\Delta}$$

where R_p and R_s are the complex reflectivities parallel and perpendicular to the plane of incidence polarized light, respectively. The ellipsometric angles Δ and Ψ are directly related to the polarizer and analyzer angles. The recorded angles were fitted in a simulation program, written in Igor Pro (Wavemetrics Inc.), based on a Fresnel model of a stack of homogeneous slabs.[41]

At the beginning of each experiment, the thickness of the alkanethiol SAM on gold was determined and kept constant throughout the experiment. The thickness of the SAM was found to be very reproducible between experiments. In those cases where Δ and Ψ were not linearly dependent, the thickness and the real part of the refractive index of the protein layer were allowed to be independent fitting parameters. For the range of angles where Δ and Ψ are linearly dependent within experimental accuracy, only the thickness was fitted, and the refractive index was assumed to be 1.40 based on results that are discussed in the text. The imaginary part of the refractive index of all layers, except the gold substrate, was always assumed to be zero.

2.6. Surface Plasmon Resonance (SPR) Spectroscopy. Binding experiments were performed in a Biacore X using homemade chips that were prepared as follows: 30 Å of Cr followed by 500 Å of Au were thermally evaporated onto glass microscope coverslips (VWR), cut to fit the Biacore cassettes and fixed to the cassettes with double-sided, water-resistant tape (3M). In a typical experiment, the chip was introduced into the instrument, which was then equilibrated at 15 °C for ~1 h in 2 M NaCl buffer. Then, the temperature was raised to 35 °C, and the instrument was equilibrated at that temperature. Next, the chip was taken out of the instrument and cooled to 4 °C, and then about 100 μL of 1 μM TRX−ELP in 2 M NaCl buffer at 4 °C was pipetted on the surface. The solution-covered chip was then transferred to room temperature, so that the temperature of the solution and chip increased to room temperature to trigger the phase transition of TRX−ELP. After equilibration for 10 min at room temperature, the chip was rinsed thrice with 2 M NaCl buffer at room temperature. Excess liquid was removed with a pipet, and the chip was immediately inserted into the Biacore instrument. Flow rates in the Biacore X were maintained at 25 μL/min to avoid formation of air bubbles on the hydrophobic surface of the collapsed ELP above its transition temperature T_c.

Anti-TRX (α-TRX) was generously provided by Prof. David Huston (Baylor College of Medicine, Houston, TX). On the basis of an extinction coefficient of 1 OD_{280} = 1.4 mg/mL for α-TRX,[47] a 1.5 μM solution of α-TRX in 2 M NaCl buffer was used for all binding studies. The volume used for one injection is limited by experimental parameters and by the relatively high flow rate, and therefore two injections of α-TRX were used to achieve saturation. In a separate experiment to determine the affinity of α-TRX for TRX, α-TRX was covalently immobilized on a CM-5 chip (Biacore) and TRX was allowed to bind to α-TRX at different solution concentrations of TRX.

2.7. Atomic Force Microscopy (AFM). Samples were taped to a glass Petri dish using water-resistant double-sided transfer tape (3M) and were cooled to 4 °C. Cooled buffer with 2 M NaCl was added to completely cover the sample, and TRX−ELP was

(41) Azzam, R. M. A.; Bashara, N. M. *Ellipsometry and Polarized Light*; North-Holland: Amsterdam, 1977.
(42) Franko, M.; Tran, C. D. *J. Phys. Chem.* **1991**, *95*, 6688−6696.
(43) *CRC Handbook of Chemistry and Physics*; CRC Press: Cleveland, OH, 1994.
(44) *International Critical Tables of Numerical Data, Physics, Chemistry and Technology, Vol. VII*; Washburn, E. W., Ed.; McGraw-Hill: New York, 1930.
(45) *Handbook of Optics*, 2nd ed.; McGraw-Hill: New York, 1995.
(46) Ohlidal, I. *J. Opt. Soc. Am. A* **1993**, *10*, 158−171.
(47) Dickason, R. R.; Edwards, R. A.; Bryan, J.; Huston, D. P. *J. Immunol. Methods* **1995**, *185*, 237−244.

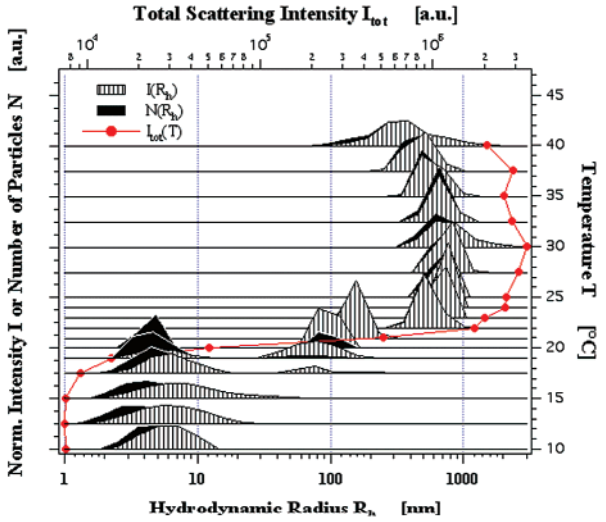

Figure 1. Hydrodynamic radii (R_h) of TRX−ELP in solution for different temperatures determined by dynamic light scattering. The relative scattering intensity as a function of particle radius $I(R)$ and the relative particle numbers $N(R)$ are both displayed in the figure, and each parameter is offset for clarity so that the curve intersects with the right axis at the appropriate temperature. The turbidity curve $I_{tot}(T)$ (top axis) as a function of temperature (right axis) is also overlaid in the figure.

then added to a final concentration of 1 μM. The sample was then allowed to warm to room temperature and to equilibrate for 15 min. The sample and Petri dish were then rinsed three times with 2 M NaCl buffer at room temperature. A Bioscope AFM (Digital Instruments) was used in contact mode at minimal force in buffer. After imaging at high ionic strength, the sample was gently rinsed at room temperature with 0.15 M NaCl buffer with a pipet without removing the dish from the setup.

3. Results

ELPs are biopolymers with the pentapeptide repeat Val-Pro-Gly-X-Gly (VPGXG), derived from a motif found in the structural protein elastin, where X can be any amino acid except Pro; the choice of X determines the phase transition temperature T_c.[35] At a solution temperature below T_c, ELPs are highly solvated and therefore soluble in aqueous solutions, but increasing the solution temperature above T_c leads to desolvation of the polypeptide and its aggregation in solution. This transition is completely reversible; when the temperature is decreased below T_c, the polypeptide is resolubilized. The transition can also be induced by a change in ionic strength, pH, and other external triggers.[36] We have previously shown that ELP fusion proteins can be produced by recombinant DNA techniques where the ELP tail is appended to the C-terminus of the protein.[33] We have also found that the phase transition behavior of the ELP is retained upon its fusion with other soluble proteins, which provides a simple method to impart stimuli responsive properties to recombinant proteins.[33]

3.1. Solution Characterization of TRX−ELP. The phase transition behavior of TRX−ELP in aqueous solution was characterized by DLS at different protein and salt concentrations by its particle size distribution and turbidity (total scattering intensity) as a function of solution temperature. A typical set of results at a TRX−ELP concentration of 1 μM in 1.25 M NaCl phosphate buffer shows the relative intensities of the scattered light associated with each particle size as a function of temperature (Figure 1). Each population of particles is stable with time at any given temperature. Additionally, intensities have been converted to relative particle numbers based on Mie scattering. The turbidity, as a function of temperature, which is simply the total scattering intensity, is also shown in Figure 1.

The turbidity curve $I_{tot}(T)$ shows a steep transition between 17.5 and 22 °C, which agrees well with turbidity measurements, independently performed in a UV−vis spectrophotometer (data not shown). This transition is also reflected in the distribution of particle sizes as a function of temperature. Up to a temperature of 17.5 °C, only a single population of particles, with a hydrodynamic radius (R_h) of ∼4−6 nm, are observed, which indicates that TRX−ELP exists as a monomer in solution. Furthermore, the ELP monomer is highly hydrated and relatively unfolded, because its R_h is approximately twice the R_h of a typical globular protein of similar molecular weight.[48] As the temperature is increased to 17.5 °C, a second population with R_h ranging from 80 to 100 nm is observed, which coexists with the monomer. When the temperature is increased above 22 °C, these particles and the monomers are no longer observed in solution and are replaced by larger aggregates with R_h of several hundred nanometers. The apparent absence of the monomers and particles with R_h of 80−100 nm may, however, be an experimental artifact, because smaller particles tend to become invisible in DLS if more than a few percent of significantly larger particles are present. The aggregation process of TRX−ELP is reversible, if the temperature is decreased (not shown), but a small number of aggregates do not readily dissolve, which makes deconvolution of the DLS results in the downward temperature cycle difficult.

3.2. Dynamic Control of Surface Immobilization of TRX−ELP. Because the bulk phase transition of ELPs is triggered by hydrophobic desolvation, we chose to study the interaction of TRX−ELP with surfaces of different hydrophobicity as a function of temperature. We chose SAMs on gold to fabricate the surfaces, because they can be easily and reproducibly prepared by chemical self-assembly from solution and enable surface properties to be systematically varied by choice of the appropriate headgroup and by the formation of mixed SAMs. Furthermore, the reflective properties of gold enable the use of surface-sensitive optical techniques such as ellipsometry and SPR to study the interfacial behavior of TRX−ELP as a function of solution conditions. We selected in situ ellipsometry as the primary analytical technique for this study, because it can measure adsorption without the need for an extrinsic label and, under certain conditions, can also detect structural changes by the change in the refractive index. In situ ellipsometry was supplemented by SPR spectroscopy and AFM.

To perform in situ ellipsometry in water, a glass cuvette was fabricated with quartz entrance and exit windows perpendicular to the beam. These windows were also designed to be free of stress-induced birefringence over a temperature range of 10−40 °C. The solution in the cuvette is thermostatted and stirred without influencing the polarization and intensity of the laser beam to achieve homogeneous conditions. Other details of the experimental conditions are described in the Experimental Section.

Figure 2 shows the ellipsometric angles Δ and Ψ for a control sample, a hydrophobic HDT SAM of HDT in standard buffer as a function of temperature from 10 to 40 °C. The ellipsometric angle Δ shows a small, systematic increase of 0.2° with temperature. This change would correspond to an apparent change in the thickness of a surface layer of about 15 Å (data not shown) over the

(48) Goodsell, D. S.; Olson, A. J. *Trends Biochem. Sci.* **1993**, *18*, 65−68.

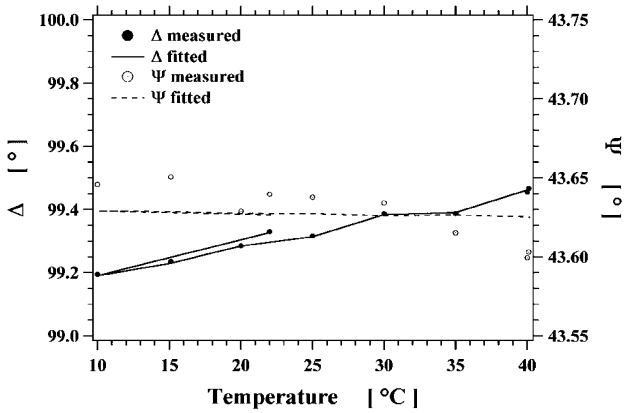

Figure 2. Ellipsometric angles Δ and Ψ of a gold surface with a CH_3-terminated SAM immersed in standard buffer solution, without any TRX−ELP, as a function of solution temperature.

10−40 °C range of temperature and is negligible compared to the thickness changes that are observed for the adsorption of TRX−ELP as a function of solution conditions. The ellipsometric angle Ψ does not change, within experimental error, as a function of temperature.

When the ELP undergoes its phase transition as a function of temperature or other solution conditions such as an increase in salt concentration, the scattering from particles in the bulk increases dramatically. Although this causes a decrease in the absolute intensity of the reflected beam, the position of the minimum in intensity in the null-ellipsometric measurement is unchanged, because the absolute intensities are not relevant in ellipsometry. This was confirmed by control experiments using an aqueous suspension of latex spheres of 200 nm and 2 μm diameter (data not shown) and is also evident from bulk exchange experiments, as described later. Scattering from the bulk does not depolarize the light, because no depolarization takes place in forward scattering, which is along the beam directions before and after the reflection at the surface. Therefore meaningful experiments can be performed above T_c, as long as particles do not enter the near-zone (≈100 Å) of the surface, and multiple scattering is not a significant contributor to the light passing through the buffer and reaching the detector. Experiments at protein concentrations much higher than 1 μM, however, are not possible with this experimental setup because of these constraints.

3.2.1. Adsorption of TRX−ELP onto a CH_3-Terminated SAM on Gold as a Function of Temperature. Gold surfaces, functionalized with a SAM of HDT, were immersed in the ellipsometer cuvette filled with standard buffer at 22 °C. After the ellipsometric angles were measured, the temperature was lowered to 10 °C, followed by the addition of TRX−ELP to a final concentration of 1 μM. The solution was held at 10 °C for 1 h, during which the thickness increased slightly due to adsorption of the fusion protein. After the first hour, the temperature was increased in steps up to a temperature of 40 °C and held constant at 40 °C for 1 h. Finally the temperature was lowered back to 10 °C. The average temperature scan rate was about 0.1 °C/min.

Figure 3 shows the ellipsometric angles Δ and Ψ as a function of temperature for a typical adsorption experiment, and experiments in Figures 5, 6, and 9 follow the same experimental sequence. The first data point at 22 °C is collected immediately after the sample has been inserted into the protein-free buffer. The buffer is then cooled to 10 °C, and a second data point is collected. Then protein is injected and several measurements are taken

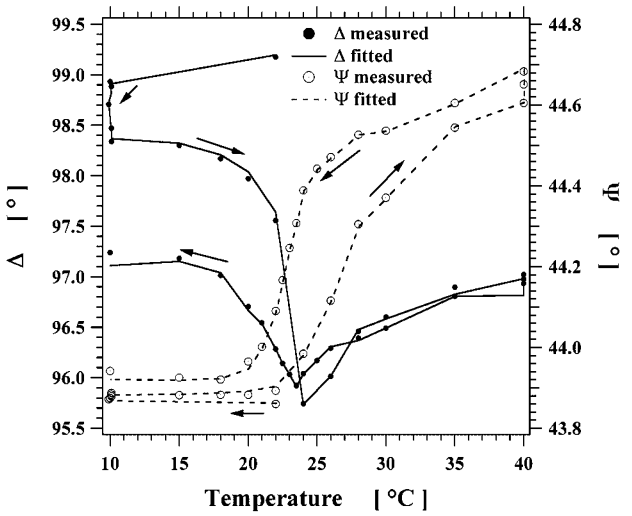

Figure 3. Ellipsometric angles Δ and Ψ as a function of temperature for a typical TRX−ELP adsorption experiment on a hydrophobic HDT SAM on gold. The first two data points (22 and 10 °C) are with buffer only. Arrows indicate the progress of the experiment.

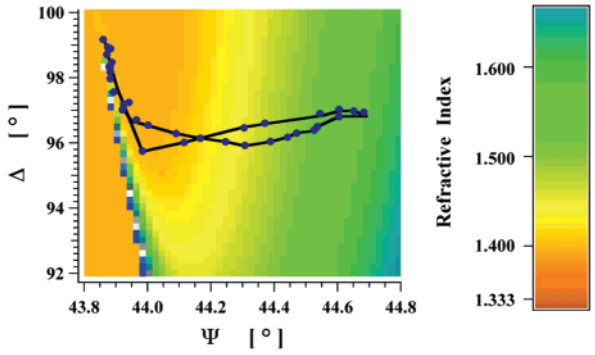

Figure 4. Ellipsometric angles Δ versus Ψ for adsorption of TRX−ELP on a hydrophobic SAM of HDT on gold as a function of solution temperature (dots, experimental data; line, fit to a Fresnel model). The curves are plotted on a background of simulated refractive indices as a function of Δ versus Ψ coded in colors. Therefore, each of the parabola-like colors of same shade represents a fixed refractive index with thickness as a parameter.

during 1 h, while small amounts of protein adsorb corresponding to a decrease in Δ from 98.9 to 98.3. After 1 h, the temperature is increased in steps. After reaching 40 °C, the temperature is held for 1 h again, before the temperature is decreased back to 10 °C. The lines are guides to the eye connecting the results of the fitting to the experimental angles. Analogous to the solution turbidity measurements, a steep change of 2.5° in Δ is observed slightly above the bulk transition temperature T_c. At the same temperature, Ψ starts to increase, while Δ goes through a minimum.

This behavior can be better understood through a Δ−Ψ plot, as shown in Figure 4. Using a Fresnel model with variable refractive index and thickness for the adsorbate layer, curves of constant refractive index are coded in false color, with thickness as the parameter within one color, starting at 0 Å at (Δ, Ψ) ≈ (99.0, 43.85) and increasing to at least 2000 Å. Each color of constant refractive index follows a parabola-like curve in the Δ−Ψ plane as the thickness is increased. Clearly, at low Ψ and high Δ angles, that is, at small thickness, only one parameter, either thickness or refractive index, can be deduced from the data, because all curves follow the same line. As the

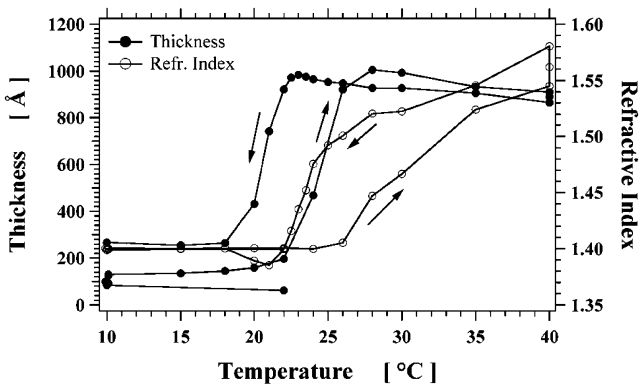

Figure 5. Thickness and refractive index of the TRX−ELP adsorbate layer as a function of temperature on a hydrophobic HDT SAM on gold as fitted to a Fresnel slab model. The first two data points (22 and 10 °C) are with buffer only. Arrows indicate the progress of the experiment.

thickness is increased, the colors spread out and Ψ and Δ become independent. The experimental data for the small, initial increase in thickness are mainly dependent on Δ, but as the thickness increases, the ellipsometric data show a sudden increase in Ψ, and a unique assignment of refractive index and thickness becomes possible. It is from this point, where the data points become nearly constant in Δ and much more dependent on Ψ, that we deduce the refractive index of 1.40 as an upper threshold for the adsorbed TRX−ELP below the transition temperature, where the Δ−Ψ curve is linear.

On the basis of a Fresnel model of homogeneous slabs and a protein refractive index of 1.40, we can determine the thickness of the adsorbed TRX−ELP layer on the hydrophobic SAM before the onset of the phase transition of the ELP. With the onset of the transition, the refractive index becomes an independent fit parameter, and both thickness and refractive index can therefore be independently determined.

Figure 5 summarizes the changes in the adsorbate layer as a function of temperature extracted from the data of Figure 3 using this fitting procedure. The first two data points, which are for protein-free buffer, have nonzero thickness, an effect seen when hydrophobic surfaces are immersed in water or buffer, which we did not subtract in our modeling. After protein is added, the thickness increases from about 150 Å at low temperatures before the onset of the transition to a final steady-state thickness in the range of 900−1000 Å at higher temperatures. The interfacial T_c, as defined by the temperature at 50% of the final, steady-state thickness, is about 25 °C on the surface, which is slightly higher than the solution T_c of 21 °C (cf. Figure 1). At a temperature 1−2 °C greater than the interfacial T_c and up to the temperature at which the surface film has reached its final thickness, the refractive index increases dramatically. This increase continues as the temperature is increased. The adsorption of TRX−ELP is reversible when the temperature is decreased. Thickness and refractive index, however, show hysteresis, and a final thickness of about 250 Å is irreversibly adsorbed on the surface after the temperature is lowered to 10 °C after one thermal cycle.

The adsorption behavior of TRX−ELP on the surface is however very sensitive to the detergent concentration in solution. We found that a very low concentration of nonionic detergent can inhibit adsorption of TRX−ELP completely. Panels A and B of Figure 6 show temperature scans on hydrophobic SAM surfaces with 50 and 10 nM Tween-20 added to the standard buffer, respectively. In 50 nM Tween 20, neither the initial adsorption of TRX−ELP (Figure 6A) nor the interfacial phase transition of TRX−ELP is observed, as seen by the lack of further adsorption when the temperature is raised from 10 to 40 °C. At a lower, 10 nM concentration of Tween-20, the surface adsorption characteristics of TRX−ELP are unchanged compared to those in a detergent-free buffer, except for a lower final refractive index for the adsorbed film at high temperatures (Figure 6B). For all the patterning experiments described in section 3.4, the solution concentration of Tween-20 was kept at 15 nM, so as to minimize the irreversible adsorption of TRX−ELP without inhibiting the interfacial phase transition. We note that the concentration of Tween-20 detergent used here is far lower than the concentration of 45 μM (0.005% v/v) of Tween-20 used for the standard binding buffer in commercial SPR instrumentation (Biacore) and is unlikely to interfere with the functional activity of most proteins.

The ability to repeatedly trigger a reversible adsorption process is desirable for a variety of applications. Repeated temperature scanning in the presence of a hydrophobic surface and standard buffer with 15 nM Tween-20, as in Figure 6C (first cycle) and Figure 6D (second cycle), shows high reproducibility of the adsorption. The transition occurs in both scans at the same temperature, the final thickness of 200 Å at the low-temperature endpoints is the same, and the high-temperature endpoints differ only by 80 Å, but the refractive index is strongly increased from 1.460 in the first to 1.574 in the second scan. The adsorption of TRX−ELP to the hydrophobic surface continues to be reversible after repeated scanning, except for an irreversibly adsorbed film of about 200 Å during the first scan, which is seen in all thermal experiments on hydrophobic surfaces. There is, however, a history effect at high temperatures indicated by the change in refractive index, even though the film thickness is basically constant.

To better understand the competition between surface adsorption and aggregation in the bulk, we investigated whether the change in the thickness of TRX−ELP in response to the environmental stimulus was caused by adsorption of TRX−ELP aggregates formed in bulk or whether the layer grows by monomer adsorption on the surface. We therefore investigated the adsorption behavior after a suspension of aggregated TRX−ELP at 40 °C was added to a standard buffer at 40 °C.

Figure 7 shows the ellipsometric angles for a hydrophobic surface as a function of time. The first data point ($t = -30$ min) is for the pure buffer at 25 °C, and the second ($t = -5$ min) is after heating to 40 °C. At $t = 0$, the protein is injected to a final concentration of 1 μM, while making sure with repeated rinsing of the vial that all the precipitate is transferred. Over the course of 2 h, an adsorbate film develops slowly with a change in Δ that is much smaller than typical values for temperature scans under these conditions, and the Ψ angle does not change significantly. Even though the range of angles does not allow a fit of both the thickness and refractive index simultaneously, the film thickness reaches a value typical of the adsorbate layers at temperatures below the transition temperature, assuming a refractive index of 1.40 (fit in Figure 7). This interpretation is supported by the film behavior, if the temperature is decreased to 25, 20, and finally 10 °C without significant changes in both ellipsometric angles ($t = 170$, 190, and 220 min, respectively).

3.2.2. Adsorption of TRX−ELP onto a COOH-Terminated SAM as a Function of Temperature. Gold surfaces, functionalized with a SAM of MUDA, were immersed in the ellipsometer cuvette filled with standard buffer at 22 °C. A thermal scan experiment was performed

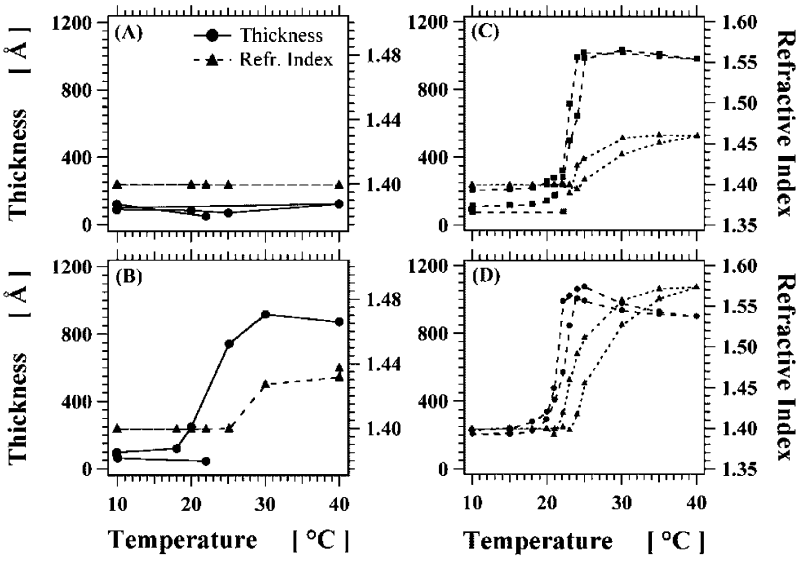

Figure 6. Effect of a nonionic detergent on the reversible surface adsorption of TRX−ELP on a hydrophobic HDT SAM on gold. Thickness and refractive index as a function of temperature for a typical buffer conditions, but containing (A) 50 nM and (B) 10 nM Tween-20 detergent. Cycling of TRX−ELP adsorption on a HDT SAM on gold with 15 nM Tween-20 in a standard buffer. Film thickness and refractive index for (C) the first cycle and (D) the second cycle.

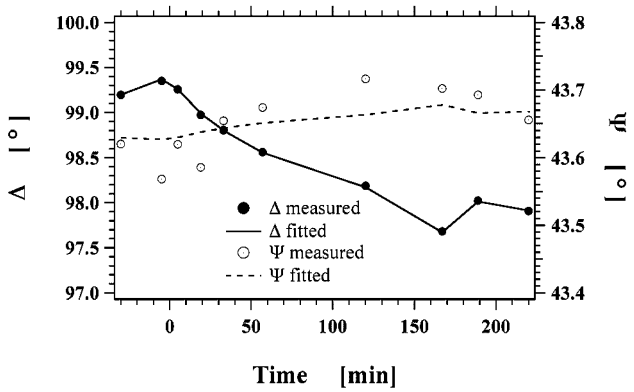

Figure 7. Ellipsometric angles as a function of time for a hydrophobic surface. Already precipitated protein is added at $t = 0$ min. The first two points before protein is added are at temperatures 22 and 40 °C, respectively. The last three points are at 25, 20, and 10 °C.

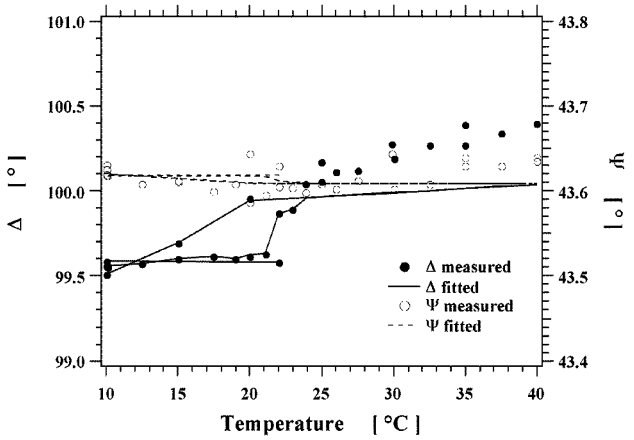

Figure 8. Ellipsometric angles Δ and Ψ as a function of temperature for a typical TRX−ELP adsorption experiment on a hydrophilic COOH-terminated SAM on gold. The first two data points (22 and 10 °C) are with buffer only.

with this surface that was identical to that described for the hydrophobic HDT SAM on gold. Figure 8 shows the change in the ellipsometric angles as a function of temperature. There is a small increase in Δ around the transition temperature, but no change in Ψ. The increase in Δ of less than 1° cannot be adequately fitted with the simple slab model as it would lead to a negative thickness. However the changes are so small that we neglect this thickness and assume that no TRX−ELP adsorbs below or above the bulk transition temperature T_c onto the hydrophilic MUDA SAM on gold. This assumption is additionally supported by the complete reversibility of the ellipsometric angles after a temperature cycle, so that no irreversibly adsorbed TRX−ELP can be seen, in contrast to a hydrophobic surface.

3.2.3. Adsorption of TRX−ELP on Hydrophobic Surfaces as a Function of Ionic Strength. Similar to their aggregation in response to increased temperature, TRX−ELP (and all ELPs in general) can also be aggregated in solution at constant temperature by the addition of NaCl. We were therefore interested in investigating whether adsorption of the ELP fusion protein to hydrophobic surfaces could be similarly controlled by changes in the solution ionic strength at constant temperature. As was the case with the temperature scans, gold surfaces functionalized with a HDT SAM were immersed in the ellipsometer cuvette filled with standard buffer at 22 °C. The initial concentration of NaCl in solution was 0.15 M, which was chosen so that the solution temperature of 22 °C is lower than T_c for TRX−ELP at a concentration of 1 μM. After adding TRX−ELP to a final concentration of 1 μM, the salt concentration in the cuvette was changed, while the temperature was kept constant at 22 °C.

Figure 9 shows the ellipsometric angles as a function of time as the NaCl concentration is cycled between 0.1 and 4 M. Also shown is the NaCl concentration in the buffer as a function of time. Due to experimental constraints, the buffer conditions were changed by adding a high ionic strength buffer in appropriate amounts until the phase transition was passed. The total protein concentration therefore varies slightly (indicated by the numbers, which are the protein concentration in μM units in Figure 9). After the transition was triggered, the bulk solution was exchanged at each step, and the bulk protein concentration was therefore always zero. At each salt concentration, the ellipsometric parameters were mea-

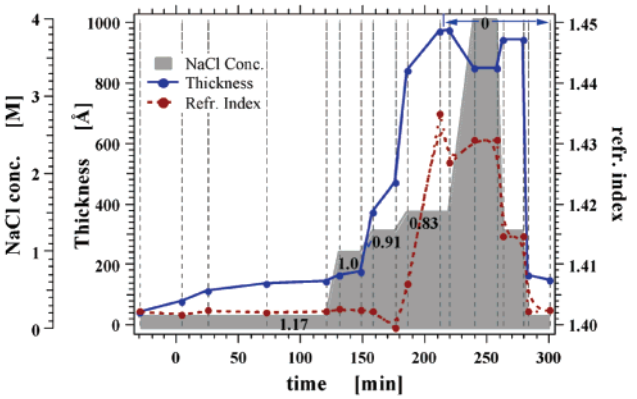

Figure 9. Thickness and refractive index fitted to the ellipsometric angles Δ and Ψ as a function of time at 22 °C for TRX−ELP adsorption on a hydrophobic surface at different salt concentrations. Underlaid in gray is the NaCl concentration as a function of time. The numbers in the graph indicate the actual bulk protein concentrations in μM. To the left of the mark at 215 min, the salt concentration was adjusted by adding high-molarity NaCl buffer, while right of the mark the buffer was completely exchanged at every step, leaving no protein in the bulk. Protein is added at $t = 0$ min.

sured immediately after the change in ionic strength and again after equilibration for 15−20 min.

As in the 1.25 M NaCl buffer at 10 °C, there is a small amount of nonspecific adsorption of TRX−ELP in the 0.15 M NaCl buffer at 22 °C during the first 120 min, which is similar to the temperature scan experiments. Even at a NaCl concentration of 1.0 M, there is little additional adsorption. At 1.25 M NaCl, about the midpoint of the transition is reached, and the thickness increases sharply and then slowly continues to increase with time. At 1.5 M NaCl concentration, the thickness quickly increases further, before slowly reaching the typical value of about 1000 Å for an adsorbed protein layer. The refractive index starts to increase too, indicating the end of the transition. At 215 min, the bulk was exchanged to a 1.5 M NaCl buffer containing no protein. While the thickness does not change, the refractive index drops, which may indicate a small loss of protein during the procedure. A further increase to 4 M salt concentration leads to a compaction of the adsorbed film, indicated by a thinner layer with higher refractive index. Reduction of the salt concentration to 1.25 M increases the thickness to about 900 Å again while the refractive index is lower than at high salt concentration, but higher than at the 1.25 M concentration on the upward scan, indicating hysteresis. Finally, at low salt concentration the protein is completely removed except for the initial adsorbate layer of about 150 Å.

3.3. Dynamic Control of Surface Functionality. Even though the environmentally sensitive TRX−ELP can be immobilized reversibly on hydrophobic surfaces, to dynamically control the surface functionality, the fusion partner has to be presented to the bulk without steric hindrance while the ELP is in the collapsed state. We used a thioredoxin specific monoclonal antibody (α-TRX) to study the accessibility of TRX to a binding partner when immobilized to the surface. We also investigated the desorption of the noncovalent complex of α-TRX and TRX−ELP from the surface upon lowering the solution temperature below the T_c. These experiments were performed in a Biacore X surface plasmon resonance instrument.

3.3.1. Binding of Anti-TRX to Immobilized TRX−ELP on a Hydrophobic Surface. TRX−ELP was immobilized outside the instrument on a hydrophobic surface in a buffer containing 2.0 M NaCl, by increasing

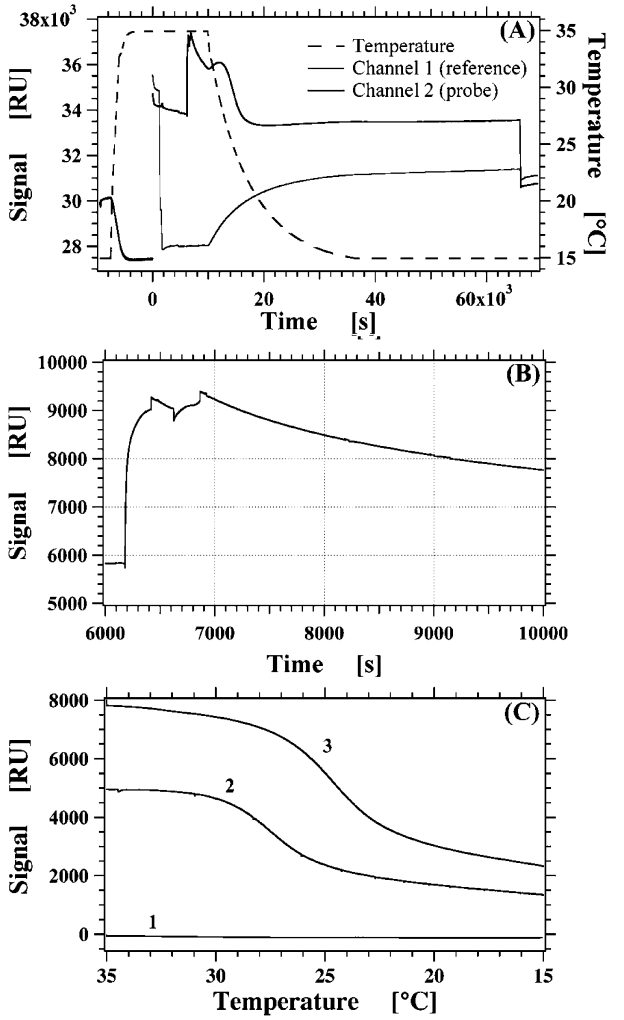

Figure 10. (A) Surface plasmon signal for the two Biacore channels and temperature as a function of time before and after ($t > 0$ s) external protein incubation. Both channels have an identical response during heating of the system before protein incubation ($t < 0$ s). After incubation of the protein outside the instrument ($t > 0$ s), channel 1 is made the reference channel by rinsing with water ($t = 500$ s) and with 0.5% SDS ($t = 1000$). α-TRX is injected twice ($t = 6200$ s). The temperature is lowered from $t = 10\,000$ s onward, and at the end of the experiment both channels are rinsed with 0.5% SDS ($t = 36\,000$ s). (B) Binding isotherm (channel 2 − channel 1) of α-TRX to an immobilized TRX−ELP layer on a hydrophobic surface. (C) Signal change (channel 1 − channel 2) during lowering of the temperature below T_c: (1) protein desorbed by water and 0.5% SDS before the temperature was lowered, (2) desorption of TRX−ELP, and (3) desorption of the complex consisting of α-TRX bound to TRX−ELP by lowering the temperature.

the temperature from 4 °C to room temperature and allowing incubation for 10 min. Figure 10A shows the surface plasmon signal of the two channels in the Biacore instrument before incubation ($t < 0$) and after incubation of the surface with α-TRX ($t > 0$). Before incubation, the hydrophobic HDT SAMs on gold exhibit approximately the same signal in both channels during the heating from 15 to 35 °C. After incubation of the surface with TRX−ELP, the signal increases by more than 8000 response units (RU), and there is a difference of 700 RU between the two channels due to small disturbances during remounting. To make channel 1 the reference channel, only this channel is rinsed with water ($t = 500$ s) and then with 0.5% sodium dodecyl sulfate (SDS) ($t = 1000$ s), which causes complete desorption of all TRX−ELP from this

channel. The resulting signal drops to about 630 RU above the signal before incubation, roughly the difference signal of 700 RU induced at $t = 0$ s. We therefore assume that channel 1 is largely free of adsorbed protein and can so be used as the reference channel. The adsorbed TRX−ELP in channel 2 meanwhile desorbs at a constant rate of 268 RU/h, which corresponds to a rate of about 4.5%/h of the original difference signal.

At $t \approx 6200$ s, the adsorbed TRX−ELP surface was incubated with a 1.5 μM α-TRX solution in 2 M NaCl buffer. This process was repeated after a brief interval to ensure complete saturation of α-TRX binding to TRX−ELP, and indeed the signal barely increased above the level of the first incubation. The surface was then left for some time to allow the unbinding process to be visible.

3.3.2. Desorption of the α-TRX/TRX−ELP Complex from a Hydrophobic Surface. With the antibody bound to the adsorbed TRX−ELP, the temperature was decreased from 35 to 15 °C to examine the phase transition triggered desorption of the bound complex. Both channels undergo a significant change in the optical response, but the difference signal is constant, if both channels have been cleared of protein (Figure 10C, curve 1). With TRX−ELP alone adsorbed to channel 2, however, the signal drops during the temperature decrease, indicating desorption of the protein (Figure 10C, curve 2). If α-TRX is additionally bound to the TRX−ELP layer, this drop is more pronounced, indicating desorption of the complex which has higher mass (Figure 10C, curve 3). In both cases, desorption below the transition temperature is not complete, similar to the in situ ellipsometry results. About 27% of the original signal for TRX−ELP alone and about 30% for the complex remain adsorbed. The slightly larger residual signal for the complex may be due to additional nonspecific adsorption of the antibody to the surface. Rinsing with 0.5% SDS, however, removes both layers.

3.4. Local Addressing of Surfaces to Achieve Reversible Patterned Surface Functionality. The previous results presented in this paper show that reversible spatial addressing of an ELP fusion protein on a surface should be feasible either by triggering the transition locally on a homogeneous surface or, alternatively, by globally triggering the transition in solution in the presence of a surface that is patterned with hydrophobic and hydrophilic regions. For experimental simplicity, we chose to demonstrate proof-of-principle of the latter.

3.4.1. Reversible Adsorption to a Hydrophobic/Hydrophilic Pattern by Temperature Change. A pattern of stripes of HDT was created with μCP of HDT on a gold surface, which was then backfilled by incubation of the surface with a solution of MUDA. Imaging ellipsometry was then used to image the adsorption of TRX−ELP as a function of solution temperature.

A sequence of images at fixed polarizer and analyzer angles, the initial ellipsometric minimum for the MUDA-modified areas, during a heating and cooling cycle is shown in Figure 11. While the pattern becomes brighter as the temperature is increased and then dims again with lower temperatures, the surrounding areas stay dark. Below the transition, the pattern is homogeneously brighter than the background due to the different thicknesses of the HDT and MUDA SAMs. Above the transition temperature, however, the pattern becomes inhomogeneous, with graininess and increased intensities along the pattern boundaries visible.

Figure 12 shows the intensities for the hydrophilic and hydrophobic areas at different temperatures taken from the images. The hydrophilic MUDA regions show no change in intensity below the T_c and very little above the

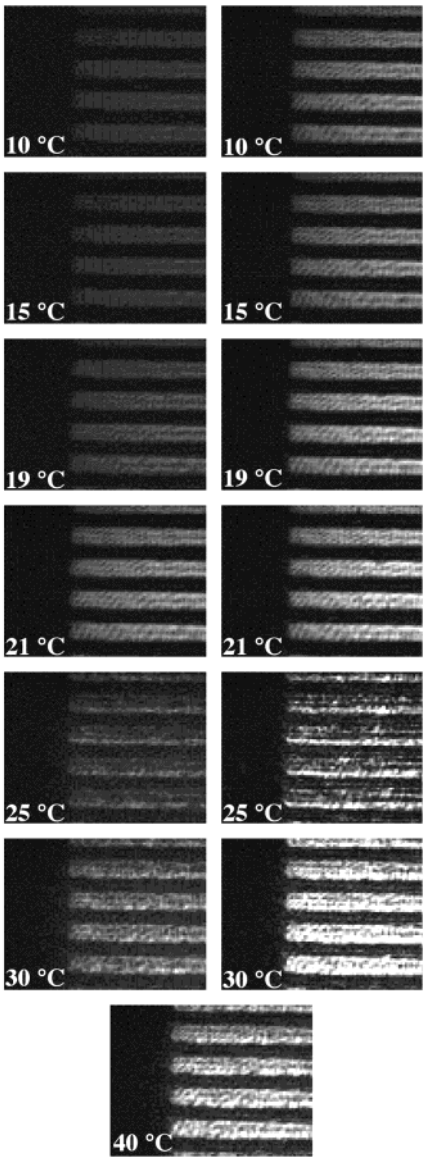

Figure 11. Imaging ellipsometer frames at different temperatures as indicated in the figure. The polarizer angles are set so that the area covered with MUDA (hydrophilic) is dark at the beginning of the experiment and then kept constant. The patterned areas are hydrophobic (HDT) and change intensity indicating adsorption and desorption of TRX−ELP. The temperature is increased from top to bottom on the left side and then decreased from bottom to top on the right side.

T_c. The small increase in intensity may be caused by imperfections in the MUDA SAM, which could have led to small amounts of protein adsorbing, or by the brightness of the patterned areas, which may increase the intensity in the MUDA SAM, since only a small part of the surface is in focus. The hydrophobic HDT pattern shows strong variation in intensity with temperature. The nonlinearity is caused by the strong nonlinear dependence of the intensity at fixed polarizer and analyzer angles on the changes of film thickness and refractive index (cf. Figures 3 and 4).

The contrast generated by TRX−ELP adsorption to patterned surfaces also allowed the adsorbed protein to be imaged by AFM even on a rough gold surface. AFM also reveals some of the submicroscopic features of the adsorbed film, which are beyond the resolution of optical techniques such as ellipsometry. To spatially address TRX−ELP onto a HDT SAM on gold, patterned against

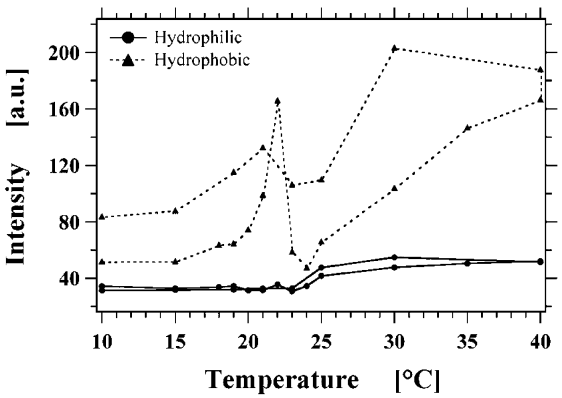

Figure 12. Intensities of the two different areas extracted from the ellipsometric images of Figure 11. While the MUDA areas show no change below the transition and little change above, the patterned HDT areas have strongly changing intensities as the temperature is changed.

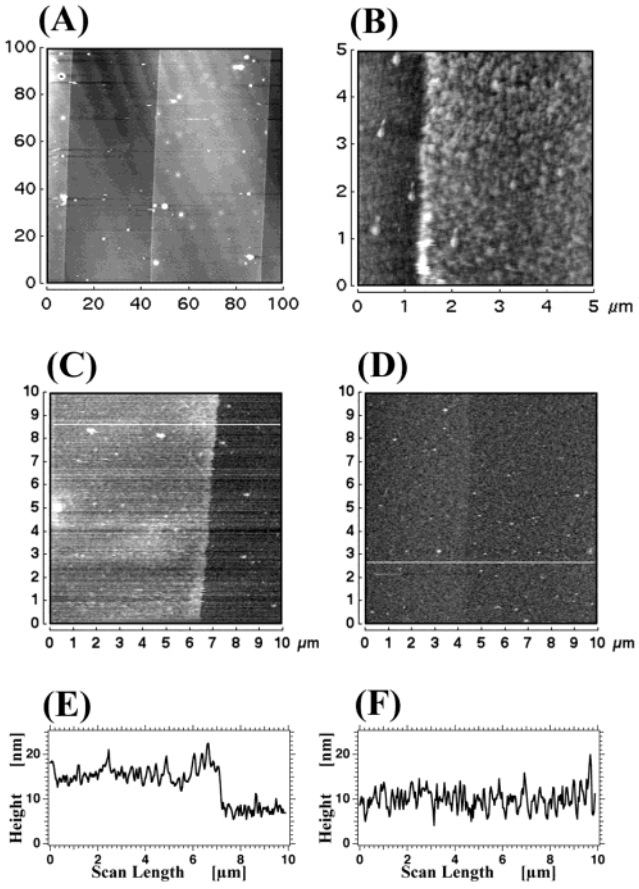

Figure 13. AFM images of patterned TRX−ELP on gold at room temperature. (A−C) Patterned TRX−ELP at room temperature in 2 M NaCl buffer above the transition. (D) Residual TRX−ELP pattern after the salt concentration has been reduced to 0.15 M NaCl. (E,F) Height profile along the white lines in (C) and (D), respectively.

a background comprising a MUDA SAM, the transition was triggered by the addition of NaCl.

The spatial addressing of TRX−ELP onto the HDT pattern in 2M NaCl can clearly be recognized in the contact mode AFM images in buffer shown in Figure 13. On a large scale, the adsorbed protein film is homogeneous over large areas but shows local "blobs", while the hydrophilic areas are nearly completely empty. On a smaller scale, however, the film is quite rough and composed of about 100−150 nm large features. After the buffer is exchanged to 150 mM NaCl, the contrast is barely recognizable, and the surface topography is dominated by the roughness of the thermally evaporated gold film.

The height of the TRX−ELP adsorbate measured by contact mode AFM in buffer is lower than measured with ellipsometry. We measured a thickness of 200−300 Å for the adsorbed TRX−ELP above the transition and about 50 Å below the transition. The difference between the film thicknesses measured by AFM and ellipsometry is probably due to compression of the loosely packed protein by the AFM tip in contact mode. Similar heights were also determined by tapping mode AFM (not shown).

4. Discussion

4.1. In Situ Ellipsometry. To the best of our knowledge, this is the first time in situ ellipsometry has been used to study physisorption of a protein in an aqueous environment over a large temperature range. Because the inverse transition dependent adsorption of ELP fusion proteins has to be conducted in aqueous solution in a cuvette with the light passing through entrance and exit windows, changes in the angle of incidence, and birefringence due to temperature-induced stress, can induce large errors. Earlier ellipsometric measurements of surface layer properties at varying temperatures were performed in a vacuum with entrance and exit windows at constant temperature,[49,50] in air through a window gap,[51,52] or with a small temperature variation in aqueous buffers.[53] While the first two methods cannot be applied to aqueous systems, in the last case birefringence was taken into account, but only in air and at room temperature.[50] For a silicon surface (not shown) and for a CH_3-terminated HDT SAM on gold, we have shown that the error induced by the experimental setup is small and allows ellipsometric measurements with high resolution to be carried out over a wide range of temperature and ionic strength. Additionally, the depolarization of the incident light at room temperature due to the cuvette was less than 0.1°. This was achieved by fabricating a special ellipsometer cuvette with stress-free windows by using thick fused silica glass with a thermal expansion coefficient of 5.5×10^{-7} °C^{-1}, compared to 7.1×10^{-6} °C^{-1} for BK7 (Melles Griot). The windows were glued together to fabricate the cuvette using silicone rubber to minimize the transmission of stress to the windows. The exit window was deliberately slightly misaligned from perfect perpendicular orientation to avoid interference due to back-reflections. The perpendicular orientation of the entrance window was controlled and adjusted after every temperature increment.

Ellipsometry is a more powerful technique than surface plasmon resonance spectroscopy or fluorescence microscopy, because it allows measurement of the film thickness and density and does not require labeling the adsorbate and therefore avoids the danger of changing the adsorption behavior due to, for instance, incorporation of hydrophobic fluorophores. We chose gold surfaces for these studies, because of the ease with which the surface can be homogeneously functionalized by solution self-assembly of alkanethiols and patterned by μCP. Ellipsometry on gold surfaces, however, has a number of disadvantages

(49) Smets, A. H. M.; Schram, D. C.; Sanden, M. C. M. v. d. *J Appl. Phys.* **2000**, *88*, 6388−6394.
(50) Landgren, M.; Jönsson, B. *J. Phys. Chem.* **1993**, *97*, 1656−1660.
(51) Kahle, O.; Wielsch, U.; Metzner, H.; Bauer, J.; Uhlig, C.; Zawatzki, C. *Thin Solid Films* **1998**, *313−314*, 803−807.
(52) Haddow, D. B.; Goruppa, A.; Whittle, J.; Short, R. D.; Kahle, O.; et al. *Chem. Mater.* **2000**, *12*, 866−868.
(53) Carlsson, F.; Elofsson, U.; Arnebrant, T.; Malmsten, M. *J. Colloid Interface Sci.* **2001**, *233*, 320−328.

because of the effect of roughness, grain size, and gaps between grains in evaporated gold films on the imaginary and real part of the refractive index. For the wavelength of 632.8 nm, surface roughness is the dominant influence on the imaginary part of the dielectric constant of gold for nonannealed gold films evaporated on smooth surfaces.[54] Our refractive index for gold, of $n = 0.20-3.558i$ ($\epsilon = -12 + 1.2I$), determined from freshly cleaned samples agrees well with the literature values for high-quality gold surfaces.[45,54] Because gold surfaces are rough, a Fresnel model of homogeneous layers determines only an effective refractive index. Additional layers can be represented by smooth slabs, ignoring the influence of the underlying randomly rough substrate, as long as each additional layer follows the underlying topography.[46] If, however, the overlayer has a different roughness that is not correlated with the underlying topography, the assumption of a smooth slab is no longer valid, and the two roughnesses have to be taken into account in combination.[46]

Null-ellipsometry (NE), however, is not capable of resolving roughness parameters. Spectroscopic ellipsometry (SE) can resolve roughness parameters,[55,56] and SE has been used to investigate protein adsorption to gold surfaces by Arwin.[57,58] In fact, a very similar dependence of the ellipsometric angles on protein adsorption was found by these investigators, resembling the L-shaped dependence seen in Figure 4. Above the interband transition of gold at about 2.5 eV ($\lambda < 500$ nm), the thickness profile could be fitted well by a monolayer of protein with slightly decreasing thickness and increasing refractive index. Below 2.5 eV ($\lambda > 500$ nm), Arwin suggests an additional interface layer characterized by the electronic interaction of gold and protein but ignores a possible roughening in the protein layer. Combining NE at 1.96 eV ($\lambda = 633$ nm) and radiolabeling, Benesch[59] showed, however, that on a smooth silicon surface amounts of adsorbed protein seem to drop at longer incubation times and are underestimated by as much as 20% compared to those for radiolabeled protein. It seems therefore more plausible that at longer adsorption times the protein layer becomes rougher, which then leads to a roughness-related effective refractive index for the protein. This is expressed in an apparent decrease in coverage seen by Benesch on silicon or a densification (decrease in thickness and increase in refractive index) as seen by Arwin on gold even above 2.5 eV. Below 2.5 eV, the additional interfacial layer, introduced by Arwin, then accounts for the mismatch of the roughness of the protein layer and the underlying roughness of the gold, which no longer have the same topography. This conclusion is supported by Aspnes,[54] who described that surface roughness was the major determinant for the effective refractive index of evaporated gold surfaces below 2.5 eV, while above 2.5 eV voids between gold grains inside the gold film are dominant and roughness is less important. Additionally, our Figure 13B shows a rough protein film, not correlated with the roughness of a gold surface. We have not converted the thickness and refractive index values to mass per area Γ using de Feijter's formula,[60] since it would hide the roughness effect and because it is not clear that a constant concentration dependence of the refractive index can be assumed through the transition.

Even though roughness in the protein film at long adsorption times limits the interpretation of the NE and possibly even SE data, the interpretation of the initial part of the adsorption curve, when mostly only Δ is changing, as an increase in thickness of the adsorbate is valid, because of little roughness in the protein film, in agreement with SE data obtained by Arwin. An additional effect can be seen in the ellipsometric data mostly on hydrophobic surfaces, which we have not corrected for. Upon insertion of the HDT−gold surfaces into the buffer, the ellipsometric angle Δ decreases below the expected value, which causes an apparent thickness of about 40−60 Å at an assumed refractive index of 1.40 (Figure 5). This effect is much smaller, about 25 Å, on hydrophilic MUDA−gold surfaces (Figure 8). On neither surface is this drop in Δ induced by an adsorbate film, since removing the buffer reproduces the values taken in air before buffer was added. An error in the refractive index of the buffer is unlikely, because the effect is seen also for water. This surface-induced layer is also responsible for the increase in Δ upon an increase in temperature, which corresponds to a slight decrease in thickness, which is not physically possible.

4.2. Mechanism of Reversible Protein Adsorption on a Hydrophobic Surface. Even though single-wavelength null-ellipsometry has its limitations, most features of the temperature- or salt-driven adsorption of TRX−ELP can be resolved with sufficient accuracy. The ellipsometric data show a clear sigmoidal behavior (Figures 5 and 6) of the adsorbed protein thickness at the assumed protein refractive index of 1.40. The thickness increase due to initial adsorption after 1 h at a low temperature of about 80 Å corresponds to close to a monolayer of fully hydrated protein (100 Å) as determined by DLS (Figures 1, 5, and 6). At higher temperatures, the thickness of the protein film of 1000 Å is clearly larger than the monomeric protein and smaller than the large aggregates of 5000−10000 Å seen in DLS. Even though a multilayer of protein could be possible, the well-defined thickness suggests a structurally well-defined aggregate (Figure 14). This explanation is supported by the appearance of particles of about 1000 Å radius at the beginning of the transition in DLS (Figure 1). The fact that these aggregates seem to disappear in bulk as soon as the larger particles appear may suggest either a specific inhibition effect on further growth induced by the surface or, more probably, a resolution problem in DLS, if two very differently sized populations coexist.

The protein adsorption due to an increase in temperature is reversible, if the temperature is lowered below the transition temperature (Figure 5). There is a hysteresis in the transition temperature, which may indicate some activation energy necessary to dissolve the supramolecular structures formed on the surface, even though each measured time point is equilibrated for at least 10 min. This hysteresis is about twice as large as the one seen in turbidity measurements.[61] Also, the final thickness of the protein adsorbate at low temperature is about 200 Å, corresponding to twice the thickness of a monolayer of fully hydrated protein. This layer, however, does not grow if the protein is cycled repeatedly (Figure 6). Similarly, if already precipitated protein is added to a solution at 40 °C free of protein, only a layer of 100 Å is created even after cooling to 10 °C (Figure 7). We therefore suspect

(54) Aspnes, D. E.; Kinsbron, E.; Bacon, D. D. *Phys. Rev. B* **1980**, *21*, 3290−3299.
(55) Aspnes, D. E.; Theeten, J. B.; Hottier, F. *Phys. Rev. B* **1979**, *20*, 3292−3302.
(56) Vedam, K. *Thin Solid Films* **1998**, *313−314*, 1−9.
(57) Martensson, J.; Arwin, H. *Langmuir* **1995**, *11*, 963−968.
(58) Arwin, H. *Thin Solid Films* **1998**, *313−314*, 764−774.
(59) Benesch, J.; Askendal, A.; Tengvall, P. *Colloids Surf., B* **2000**, *18*, 71−81.
(60) de Feijter, J. A.; Benjamins, J.; Veer, F. A. *Biopolymers* **1978**, *17*, 1759−1772.
(61) Meyer, D. E.; Kong, G. A.; Dewhirst, M. W.; Zalutsky, M. R.; Chilkoti, A. *Cancer Res.* **2001**, *61*, 1548−1554.

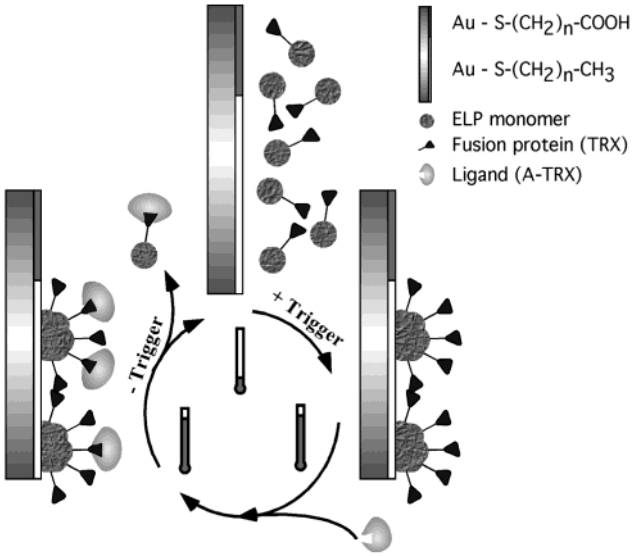

Figure 14. Schematic of thermodynamically reversible addressing of a static surface pattern to achieve a functional pattern. Adsorption of TRX−ELP in response to triggering the ELP phase transition proceeds by formation of semimicelles of TRX−ELP. The thus immobilized fusion partner can be recognized by a ligand, and the complex resolubilized when the trigger is inverted.

that the first layer consists of protein in a different state than the second layer, even though both are no longer soluble. A transition in thickness and density in this adsorbed protein monolayer or bilayer upon heating and cooling through the transition temperature, as seen by Carlsson,[53] could not be found (not shown), because the thickness and refractive index parameters are nearly linearly dependent and cannot be resolved on gold surfaces.

Taken together, the ellipsometry and AFM results suggest that upon incubation of a hydrophobic surface with an aqueous solution of TRX−ELP below the T_c of the ELP, the adsorption of a monolayer of TRX−ELP is the first event that rapidly proceeds to steady state (Figure 14). As the solution temperature is raised to the T_c, an increase in film thickness is observed that is caused by the nucleation of ELP aggregates on the adsorbed TRX−ELP. The aggregates grow as the temperature is raised further but are limited to a terminal size that corresponds to an effective film thickness of about 1000 Å by steric limitations on the growth of aggregates in two dimensions (Figure 14). In contrast, in semidilute solutions, these aggregates can grow to a much larger size, because of the lack of steric constraints.

Similar to the effect of temperature, the adsorption of TRX−ELP can also be triggered by a change in NaCl concentration. Overall, the mechanism of TRX−ELP adsorption appears to be similar to that triggered by a temperature change with some notable differences. Even though the adsorption and desorption behavior in salt and temperature scans is very similar, the thickness of the final irreversibly adsorbed layer at low salt concentration is equal to the thickness of the initial adsorption, corresponding to only one monolayer of TRX−ELP of 100 Å. These results suggest that the degree of reversibility as a function of isothermally cycling the desorption process is somewhat better when the phase transition is triggered by salt, rather than temperature, because thermal cycling presumably results in a small but significant degree of protein unfolding at the hydrophobic surface. The salt scan also shows (Figure 9) that there is a rearrangement of the protein film at high salt concentrations. At 4 M NaCl with no protein in solution, the protein adsorbed at the surface undergoes a thickness decrease while the refractive index increases. This corresponds to a compaction within the film, which cannot be solely explained by an increase in surface roughness. This effect is reversed when the ionic strength is decreased. We suggest that this compaction is cause by additional desolvation of the aggregates due to a "salting out" effect that is distinct from the behavior that accompanies the phase transition of the ELP during its aggregation.

4.3. Functionality of the Adsorbed Protein Film on Hydrophobic Surfaces. To show that the adsorbed TRX−ELP has produced a functional surface, we measured the binding of the monoclonal antibody to TRX. A Biacore surface plasmon instrument is better suited for these experiments than ellipsometry, because its temporal resolution is optimized for surface binding kinetics and because the objective of these experiments is not the determination of absolute values for thickness or refractive index. Even though the current experiments allow only a rough estimate of the on-rate for the α-TRX binding to TRX, both the on- and off-rates are within a reasonable range to ensure that recognition is occurring and TRX is not buried inside the TRX−ELP film. Surface plasmon resonance showed that the recognition event does not hinder desorption of the protein film, and the whole complex can be resolubilized by lowering the solution temperature below the T_c of TRX−ELP. However, we note that TRX is a very soluble protein, and more hydrophobic fusion proteins may be less exposed in an ELP-anchored surface layer. The hydrophobicity of the fusion protein influences the transition temperature[33] and could lead to a partial burying in the ELP layer. Studies investigating these questions are currently in progress.

4.4. Inhibition of Protein Adsorption on Hydrophilic Surfaces and Contrast Creation in Patterns. On hydrophilic MUDA−gold surfaces, the adsorption of protein can be inhibited. No adsorption occurs during an incubation at constant low temperature or during heating (Figure 8). On the basis of the clear difference in the temperature-triggered adsorption behavior of TRX−ELP on hydrophobic and hydrophilic surfaces, a patterned surface of hydrophilic and hydrophobic areas can be used to create a surface that is patterned with the fusion protein (Figures 11, 12 and 13). In contrast to most other methods to pattern proteins,[9,13,20−23,27,62] the pattern created by TRAP can be "erased" by reversing the interfacial phase transition and resolubilizing the adsorbed protein. The surface is then available for a new adsorption step. Even though we have shown the reversibility of this process only for adsorption triggered by temperature and ionic strength in this paper, other triggers such as ionic strength, electrochemical potential, osmotic pressure, and light can be used. In particular, triggers such as light and electrochemical potential can induce the adsorption transition at the micron scale so as to address individual areas within a pattern, so that selective addressing of specified regions in the pattern can be achieved. In this context, it is very important to know that the adsorbate will not be removed upon rinsing (Figures 9 and 10) and that precipitated protein will not adsorb to a surface, except for a monolayer on a bare surface, which would not interfere with the triggered, reversible adsorption process (Figure 7).

(62) Mrksich, M.; Whitesides, G. M. *Annu. Rev. Biophys. Biomol. Struct.* **1996**, *25*, 55−78.

5. Conclusions

We have shown that a stimuli responsive ELP can be used to trigger the adsorption of a fusion protein to a physically patterned surface template. The adsorbed fusion protein is oriented such that it can bind its affinity partner from solution, and the bound complex can be resolubilized when the trigger is reversed. Together, the results presented in this paper demonstrate proof-of-principle of three out of the four steps necessary to create a fully dynamic patterned surface: (1) writing information by adsorption of a protein using an ELP, (2) reading information by a recognition event, and (3) erasing information to prepare for a new write process by resolubilizing the ELP with its fusion protein as well as possible bound ligands. Furthermore, the TRX−ELP system has also enabled us to demonstrate that in situ ellipsometry can be used to extract valuable information from a solid−liquid interface over a fairly wide temperature range.

Future research will examine the generality of this method with a variety of ELP fusion proteins as a function of surface chemistry including the use of different protein-resistant surfaces in the background. Furthermore, although we have used temperature and ionic strength as triggers to demonstrate proof-of-principle of TRAP, there are a variety of other triggers that can be used to adsorb the ELP onto a surface pattern by TRAP, including electrochemical and optical triggers. The incorporation of multiple triggers would enable the formation of patterns with multiple functionality, which could be separately switched on and off. In conclusion, we believe that TRAP is likely to be a useful method to spatially address proteins and their noncovalent complexes dynamically to surfaces and will have diverse applications in the fabrication of "smart" (stimuli responsive) biomaterials, biosensors, and proteomic arrays.

Acknowledgment. This research was supported by a grant from the National Institutes of Health (R01-GM-61232) to A.C.

LA026359D